Volume 7 | Number 6 | 14 February 2019 | Pages 1401–1728

Journal of Materials Chemistry C

Materials for optical, magnetic and electronic devices

rsc.li/materials-c

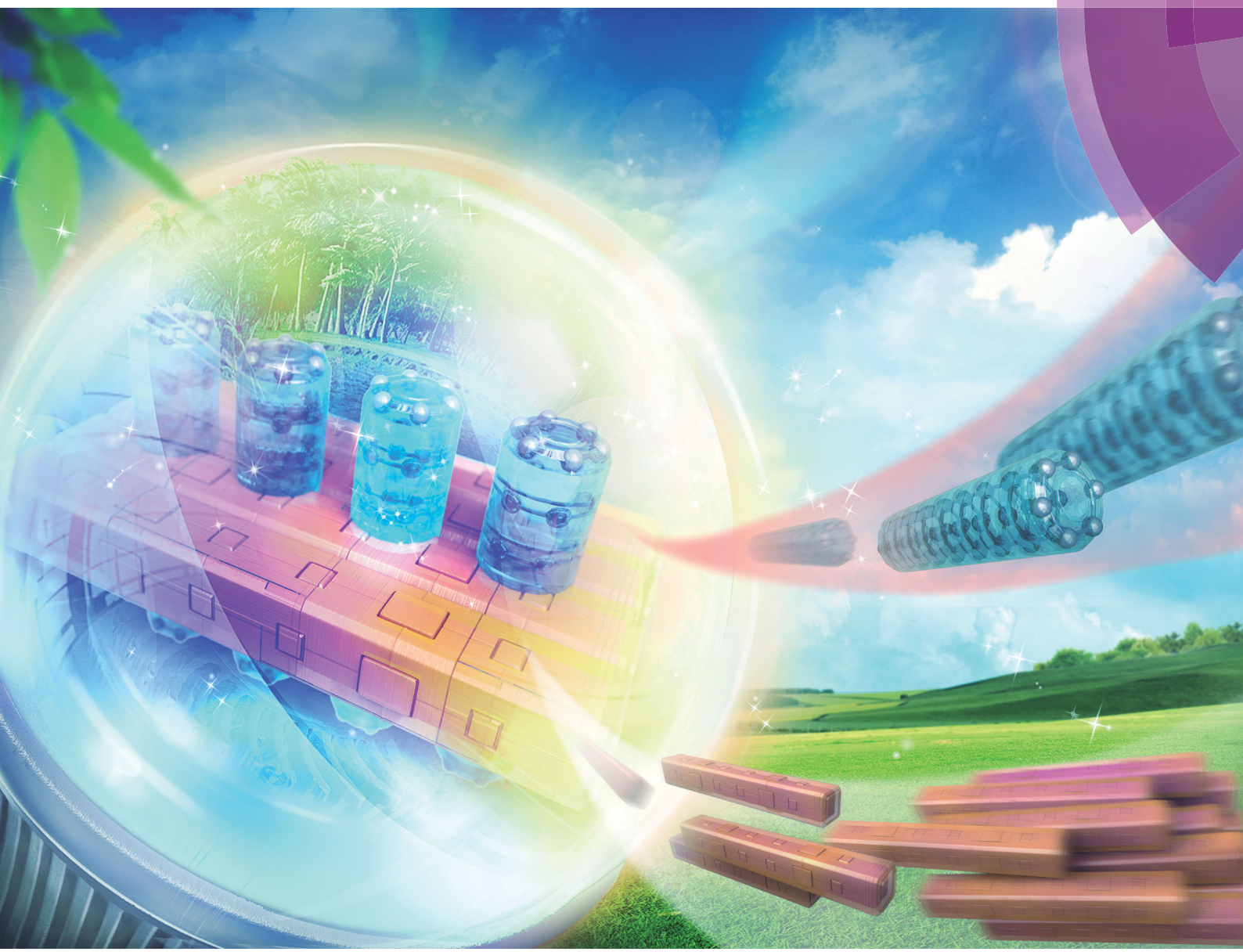

ISSN 2050-7526

ROYAL SOCIETY OF CHEMISTRY | Celebrating IYPT 2019

PAPER

Jing Li *et al.*

Strongly luminescent inorganic–organic hybrid semiconductors with tunable white light emissions by doping

Journal of Materials Chemistry C

PAPER

View Article Online
View Journal | View Issue

Cite this: J. Mater. Chem. C, 2019, 7, 1484

Strongly luminescent inorganic–organic hybrid semiconductors with tunable white light emissions by doping†

Wei Liu, [ab] Debasis Banerjee,[b] Fang Lin[a] and Jing Li *[ba]

Received 4th October 2018,
Accepted 3rd December 2018

DOI: 10.1039/c8tc05020a

rsc.li/materials-c

A series of copper bromide based inorganic–organic hybrid semiconductors have been synthesized by doping a trace amount of a secondary ligand into their parent structures. Upon near-ultraviolet excitation, these structures emit broadband bluish (''cold'') to yellowish (''warm'') white light. The color temperature can be systematically tuned by controlling the type and amount of the dopant. Our studies show that the observed white emission is emitted directly from the doped sample, and is not a combined effect from mixed phases. The internal quantum yields (IQYs) of these white-light-emitting hybrids are as high as 68%, which are significantly higher than those of most direct white-light-emitting phosphors reported to date. In addition, these copper halide staircase chain based hybrid structures exhibit interesting thermochromic luminescence. The high quantum efficiencies coupled with facile and low-cost synthesis and strong optical tunability of this materials group suggest its considerable promise for lighting-related applications.

Introduction

Energy-efficient white-light-emitting-diodes (WLEDs) are commonly produced by coating blue LED chips with blue-excitable phosphors. Such systems are regarded as phosphor-converted WLEDs (pc-WLEDs).[1,2] A simplest pc-WLED makes use of a yellow phosphor, cerium-doped yttrium aluminium garnet (YAG:Ce). However, light emitted from this device typically lacks the lower energy (red) emission, resulting in an elevated correlated color temperature (CCT) that is too ''cold'' for indoor illumination.[1,3] An alternative approach is the excitation of a direct white light-emitting phosphor using a near ultraviolet LED chip. Such phosphors are typically a blend of several monochromic emitters. This design has several advantages such as better light quality, facile device fabrication, *etc.*[4–6] However, there are also disadvantages including significant self-absorption and color change due to the decomposition of one component in the blends.[7–10] Besides these issues, nearly all commercial phosphors in today's market contain rare-earth elements (REEs), which bring up potential supply, cost, and environmental issues.[11,12]

In the recent years, single-phase, non-rare-earth, direct white-light-emitting phosphors have been developed and are attracting increasing attention due to their considerable potential for lighting-related applications.[13–25] For example, II–VI (*e.g.* Zn, Cd and S, and Se) group based nano-crystal quantum dots (QDs) of very small size can generate white light.[26–28] However, their internal quantum yields (IQYs) are generally low. Their emissions are highly dependent on the particle sizes, which also require complicated synthesis procedures. These drawbacks limit their practical use. Inorganic–organic hybrid semiconductors are a unique family of semiconductor bulk materials that exhibit enhanced properties with respect to their parent structures.[29–36] Unique properties, especially luminescence, have emerged as a result of combining both the inorganic and organic components in a single crystal lattice.[14,37–40] The structures built on II–VI group based semiconductors and alkyl-amines emit white light in their bulk phases. Their IQYs reach 37% upon Mn^{2+} doping.[14,41,42] Layered halide perovskites, on the other hand, exhibit intrinsic white light emission with an IQY of 9%.[37,43,44] However, compared to the IQYs of commercial phosphors, which are usually higher than 80%, the photoluminescence efficiency of these structures needs to be further improved for practical applications.

Our recent studies on I–VII binary metal halide (Cu, Ag and I, Br, and Cl) based inorganic–organic hybrid semiconductors demonstrate their strong potential as general lighting phosphors.[38,45–47] This family of compounds have a number of advantages compared to commercial and other phosphor classes, such as strong luminescence, earth-abundance, REE-free, and facile one-step synthesis.

[a] Hoffmann Institute of Advanced Materials, Shenzhen Polytechnic, 7098 Liuxian Blvd, Nanshan District, Shenzhen, 518055, China
[b] Department of Chemistry and Chemical Biology, Rutgers University, 610 Taylor Road, Piscataway, NJ, 08854, USA. E-mail: jingli@rutgers.edu

† Electronic supplementary information (ESI) available: Crystal images, structural plots, PXRD patterns, TGA data, DFT calculation results, UV-vis absorption spectra and PL spectra. CCDC 1506741, 1506742 and 1506745. For ESI and crystallographic data in CIF or other electronic format see DOI: 10.1039/c8tc05020a

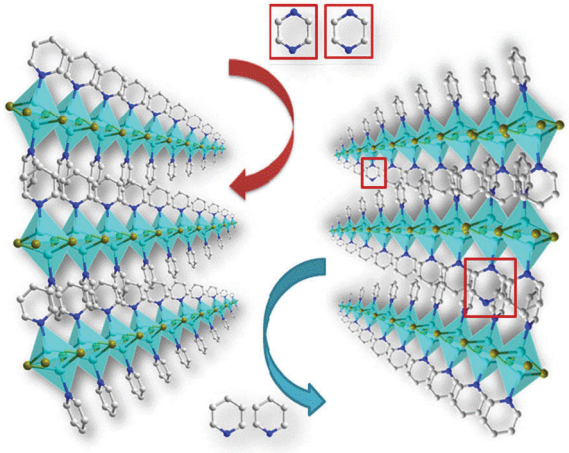

Fig. 1 Schematic illustration of the ligand doping approach in designing white emitting 1D-CuBr(py)$_{1-x}$(pz)$_x$ compounds.

The emission profiles of nearly all of these structures are single-band type, with a full width at half maximum (FWHM) of around 100 nm.[48,49] Broadened emission spectra can be obtained by doping a secondary ligand onto pristine hybrids.[38] Herein, we report a series of one dimensional (1D) staircase chain-like copper(I) bromide based inorganic–organic hybrid compounds with the general formula 1D-CuBr(pyridine)$_{1-x}$(pyrazine derivatives)$_x$ ($x < 0.01$), where pyrazine (pz) derivatives are the dopants (Fig. 1). These doped compounds exhibit tunable white light emission as well as significantly enhanced IQYs, a 6-fold improvement compared to previously reported copper iodide based analogues.[38] A comprehensive analysis has been done by varying the doping amount and by modifying the dopants with different functional groups. The results demonstrate that the light temperature of the doped compounds is adjustable. Bluish ("cold") to yellowish ("warm") white light from the single crystals of these structures was observed, indicating that the white light is emitted directly from the doped bulk materials (Fig. 2). Moreover, we observed reversible thermochromic behavior in all white-light-emitting compounds. This behavior has never been reported previously for copper halide staircase chain based structures. The advantages of high IQYs, facile synthesis and optical tunability make this type of phosphor promising candidates as lighting phosphors, and their thermochromic behavior may lead to new applications.

Results and discussion

Attempts to synthesize copper bromide based hybrid semiconductors led to the formation of compounds **1–4**. They are all copper bromide staircase chain based structures (Fig. S4–S9, ESI†). Important crystallographic data of these compounds are listed in Table 1. Their phase purities were evaluated and confirmed by elemental analysis (Table S1, ESI†). Optical absorption spectra for compounds **1–4** were recorded at room temperature and converted to the Kubelka–Munk function (Fig. S12, ESI†). Their band gaps were estimated using their absorption edges, and are 3.1, 2.8, 2.7 and 2.5 eV, respectively.

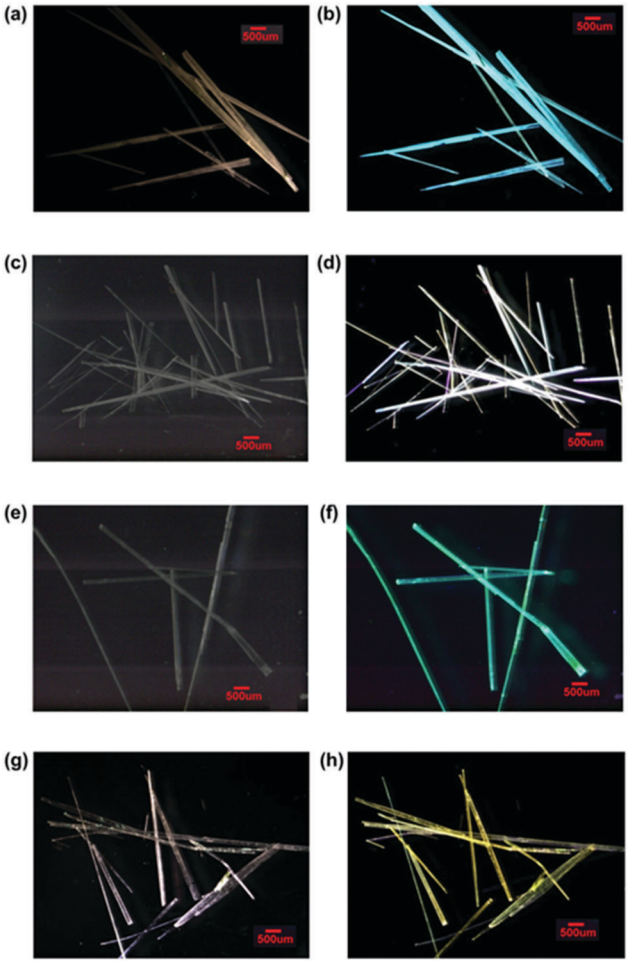

Fig. 2 Single crystals of **2** (a), **2c** (c), **2f** (e), **2g** (g) under natural light and **2** (b), **2c** (d), **2f** (f), **2g** (h) under UV light (365 nm).

Table 1 Summary of the crystal data of new 1D-CuBr(L) structures (L = py functionalized ligand)

Compound	1D-CuBr (3,5-dm-py) (**1**)	1D-CuBr (3-Cl-py) (**3**)	1D-CuBr (3-Br-py) (**4**)
Empirical formula	C_7H_9BrCuN	$C_5H_4BrClCuN$	$C_5H_4Br_2CuN$
FW	250.60	256.99	301.44
Space group	$C2/c$	$P2_1/n$	$P2_1/n$
a (Å)	13.910(17)	8.7438(19)	8.720(9)
b (Å)	15.111(18)	3.9296(9)	3.933(4)
c (Å)	8.107(10)	21.002(5)	21.11(2)
A (°)	90.00	90.00	90.00
B (°)	99.455(17)	100.837(3)	100.603(13)
γ (°)	90.00	90.00	90.00
V (Å^3)	1681(4)	708.7(3)	711.6(12)
Z	8	4	4
T (K)	298(2)	298(2)	298(2)
λ (Å)	0.71073	0.71073	0.71073
R_1	0.0396	0.0306	0.0479
wR_2	0.0973	0.0817	0.1207
CCDC	1506745	1506742	1506741

This trend corresponds to the decreasing LUMO energies of the organic ligands in the structures, which are −1.039, −1.120, −1.473 and −1.492 eV for 3,5-dm-py, py, 3-Cl-py and 3-Br-py, respectively (Table S2, ESI†). As shown in Fig. S15 and Table S3 (ESI†),

these structures emit strongly in the visible light region and their emission colors range from blue to green. Their emission spectra are all single-band type, with an average full width at half maximum (FWHM) of around 100 nm. Their emission energies are related to their band gap values and the LUMO energies of the incorporated ligands. The internal quantum yields (IQYs) of **1–4** were determined at room temperature, and the values obtained with 360 nm as the excitation wavelength are 56%, 48%, 27% and 21% for **1**, **2**, **3** and **4**, respectively. These results demonstrate that the varying functional groups on the py ligands significantly influence the quantum yields of the hybrid structures. Electron donating groups, such as methyl groups, enhance the emission, while electron-withdrawing groups, such as chlorine or bromine, lower the emission efficiency. The structures' band gaps, emission energies, IQY and ligand LUMO energies are highly related to each other and are in agreement with our previous studies on 1D-CuI(L). The optical properties of these structures can be tuned by ligand design and selection.

Compound **2** or 1D-CuBr(py) (space group $P2_1$) was chosen as the parent structure for the doping study.[50] It exhibits intense blue-green emission (λ_{em} = 494 nm) under near-UV excitation (λ_{ex} = 360 nm) with an IQY of 48%. In the case of the parent structure, adding a trace amount of pz afforded doped products 1D-CuBr(py)$_{1-x}$(pz)$_x$ ($x < 0.01$) (compounds **2a–2d**). The PXRD analysis confirmed that the crystal structures of these doped samples remain the same (Fig. 3a). Photoluminescence measurements of the doped samples show that their emissions change significantly compared to that of the parent structure (Fig. 3c). The blue-green emission band from their parent structure remains in the higher energy (HE) region, while the second band emerges in the spectra in the lower energy (LE) region, resulting from doping. The HE and LE bands combine to give a broad emission spanning over the entire visible light region (400–700 nm). Centimeter-long single crystals of the doped samples were obtained by a layering approach and all optical measurements of the doped samples were from the single-phase samples. It was observed that the white light is emitted directly from the single crystals, suggesting that it is a bulk property of the material. We also grinded the single crystals of 1D-CuBr(py)$_{1-x}$(pz)$_x$ (x = 0.0012) into fine powder. No changes in the emission were observed before and after grinding, confirming that the luminescence is not a surface property.

The absorption spectra for doped structures **2a–2h** were collected and all show a single, sharp absorption edge, indicating that they are single-phase compounds (Fig. S13, ESI†). All of the doped compounds have nearly the same band gap values as that of their parent structure 1D-CuBr(py). The possible impurities from the dopants under these conditions are 2D-CuBr(L)$_{0.5}$ (Fig. S5b, ESI†), which have band gaps around 2.0 eV, significantly lower than that of 1D-CuBr(py).[51] However, no absorption at the lower energy part was observed in any of the spectra of the doped structures. This confirms that the second bidentate ligands have been doped into the parent structure, and are not forming the second impurity phase. Further increasing the doping level to

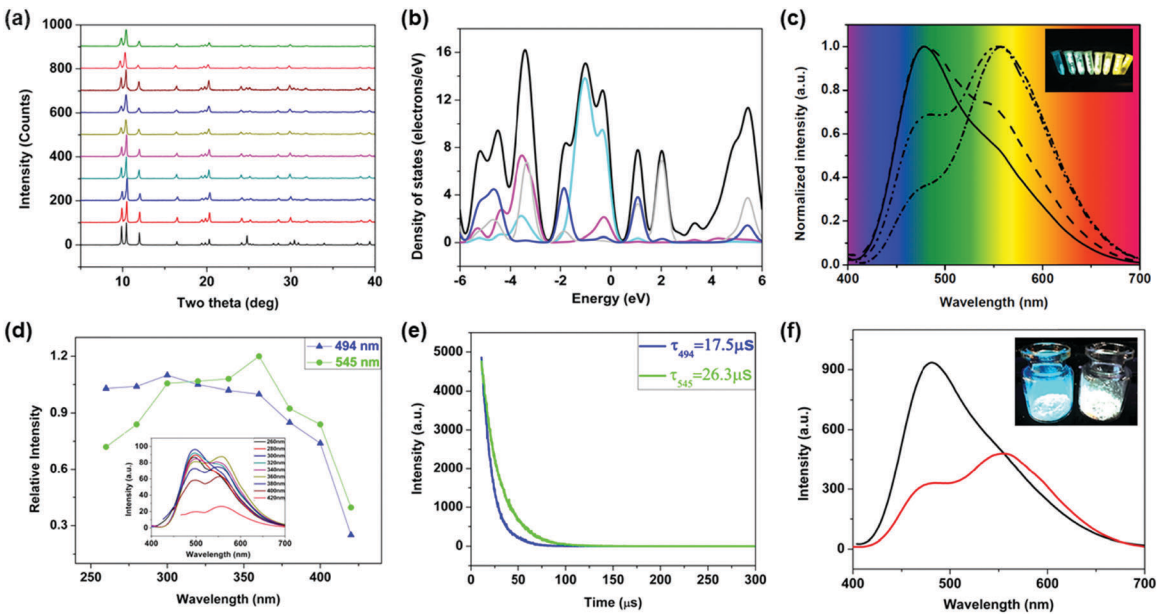

Fig. 3 (a) PXRD patterns of the parent and doped structures of 1D-CuBr(py) compared with their simulated patterns. From bottom to top: simulated **2**, as-synthesized **2**, and as-synthesized **2a–2h**. The dopant concentrations are listed in Table 2. (b) Calculated density of states (DOS) of 1D-CuBr(py) (**2**) by the DFT method: total DOS (black); Cu 3d orbitals (light blue); Br 4p orbitals (pink); C 2p orbitals (grey); and N 2p orbitals (blue). (c) Photoluminescence spectra of **2a** (solid), **2b** (dash), **2c** (dash dot dot) and **2d** (short dash dot). Inset: Photo images of the doped samples under UV light. Samples from left to right: parent 1D-CuBr(py), 0.004%, 0.008%, 0.02%, 0.05%, 0.07%, 0.12%, 0.32% pz doped 1D-CuBr(py). λ_{ex} = 365 nm. (d) Relative intensities of the HE band at 494 nm (blue) and the LE band at 545 nm (green), respectively, for **2c**, as a function of excitation wavelengths. The intensity of the HE band at 360 nm is set to 1. Inset: PL spectra of **2c** at various excitation wavelengths. (e) Luminescence decay spectra of **2c** at 494 nm (blue) and 545 nm (green). λ_{ex} = 360 nm. (f) PL spectra of **2c** at room temperature (red) and at 77 K (black). Inset: Images of **2c** taken immediately after removing the sample from liquid nitrogen (left) and at room temperature (right).

x = 0.01 leads to the formation of the second phase, identified using the UV-vis absorption spectra as a new absorption band appeared in addition to that of 2D-CuBr(pz)$_{0.5}$ (Fig. S14, ESI†). Therefore, we keep the doping amount significantly lower than 1% to ensure their single phase purity.

Upon varying the doping level of pz, from 0.05% to 0.32% molar ratio to that of py, the peak positions of the HE and LE bands remain unchanged while their intensities vary based on the doping level. With an increase in the doping amount, we observe a gradual intensity decrease of the HE band along with an intensity increase of the LE band. When the doping level reaches 0.32%, the HE is almost totally quenched, resulting in intense ''yellowish'' white light.

The intense blue-green emission of the parent structure 1D-CuBr(py) is primarily attributed to a combination of metal-to-ligand charge-transfer (MLCT) and halide-to-ligand charge transfer (XLCT) luminescence mechanism, as confirmed by Density Functional Theory (DFT) calculations (Fig. 3b and Fig. S11, ESI†). The band gap and emission energy of this type of structure are correlated to the LUMO energy of the ligand. Further calculations of the LUMO energies show that pz has a distinctly lower energy (−1.857 eV) compared to that of py (−1.120 eV), indicating that the parent ligand and the dopant might be responsible for the dual emissions (Table S2, ESI†). To understand this, we kept the parent ligand py, and changed the pz to pz derivatives (2-et-pz, 2-me-pz, 2-Cl-pz, 2-Br-pz) with different LUMO energies. Single crystals of **2e–2h** were obtained with these dopants, and PXRD analysis along with a UV-vis absorption experiment was conducted to confirm their phase correctness and purity. Based on their photoluminescence measurements, all compounds show a two-band type spectrum (Fig. S16, ESI†). The emission energies of the HE band remain constant for all of them, proving that the HE band is from the parent ligand py. The energies of the LE band, however, changes accordingly based on the LUMO energies of the dopants, providing strong evidence that the LE band is originated from the dopants.

Furthermore, the relative intensities of the HE and LE bands at various excitation wavelengths were studied (Fig. 3d). The observation of their excitation-wavelength dependent emissions suggests that the HE band and the LE band are from the isolated luminous centers. Time-resolved PL measurements were conducted on the doped sample at an excitation wavelength of 360 nm at the emission maximum of the two bands. The lifetime values for 495 nm and 550 nm emissions are 17.5 μs and 26.3 μs, respectively (Fig. 3e). The difference in the lifetime values reflects their different excited states.

The temperature-dependent emission spectra of the doped samples show that they all display thermochromic behavior (Fig. 3f). The intensity of the LE band completely quenched when the sample was dipped in liquid nitrogen (77 K), while the intensity of the HE band became much stronger. After removing the crystals from liquid nitrogen, the initial emission intensities of the two bands regained as the sample temperature returned to RT, indicating that the thermochromic luminescence is fully reversible. Though thermochromic behavior for copper halide cubane cluster-based hybrid materials has been well studied and is attributed to the short Cu–Cu bond distances (smaller than 2.8 Å),[48,52–54] as far as we are aware, such behavior has not been reported for staircase chain based structures. For example, a typical cubane cluster, 0D-$Cu_4I_4(py)_4$, exhibits LE (yellow) emission at room temperature originated from ''cluster centered'' (CC) luminescence, and at low temperature (77 K), the LE emission is quenched and HE (blue) emission emerges as a combination of MLCT and XLCT.[48] The LE band emission in doped 1D-CuBr(py) samples is similar to that of cubane based structures, indicating that they might also be attributed to the CC luminescence mechanism. Single crystal X-ray diffraction is not capable of providing an answer as the doping level is too low to form an ordered structure. We also noted that the dopants must be multidentate ligands in order to achieve the broadening effect of the spectra. Other multidentate ligands, including pyrimidine (pm) and 1,3,5-triazine (tz), exhibit a similar behavior to that of pz derivatives (Fig. S17, ESI†). However, upon replacing these dopants with monodentate ligands having lower LUMO energies, such as 3-cyano-py and 4-cyano-py (Table S2, ESI†), no broadening effect was observed. The full understanding of the broadening effect through doping is still limited, and a further in-depth investigation of the luminescence mechanism is now underway.

The direct application of these white-lighting-emitting materials is their use as lighting phosphors. The quality of the white light from these phosphors is readily tunable by selecting suitable dopants and doping amount. The performance of the doped compounds as lighting phosphors was evaluated by measuring their IQY, CIE (International Commission on Illumination) color coordinates, Color Rendering Index (CRI) and CCT under excitation with near-ultraviolet light (365 nm) and the results are summarized in Table 2. It is interesting to observe that the IQYs of most doped structures are higher than that of their parent structure, with the highest IQY value of 68% for compound **2e**. Compared to other reported direct white light emitting phosphors, which generally suffer from low IQYs, most of these compounds have IQYs higher than 60%. More interestingly, their color temperature can also be tuned, from bluish (cold) to yellowish (warm) white light, as evident from their CCT values (Fig. 4). The current commercial white light LEDs made from YAG:Ce produce ''cold'' white light with CCT values higher than 5000 K, which may not be suitable for indoor illumination.[1] The color temperatures of the doped 1D-CuBr(py) samples, on the other hand, range from 3360 K to 5792 K, making these materials usable under various environments.

Moreover, the water stability of these materials ensures their solution processability. Using a commercial binder, they can be easily coated onto different substrates. Prototype WLED bulbs were fabricated by coating 5 mm 365 nm LED chips with doped samples having various CCT values. These bulbs display white light from ''cold'' to ''warm'' as their CCT values decrease from 5024 K to 3360 K (Fig. 4).

Experimental

Materials

CuBr (98%, Alfa Aesar), KBr (>99%, Alfa Aesar), acetonitrile (>99%, Alfa Aesar), pyridine (py, >99%, Alfa Aesar), 3,5-dimethylpyridine

Table 2 Summary of the composition and optical properties of the white-light-emitting structures

#	Dopant	Doping amount	Band gap (eV)	λ_{em} (nm) (298 K)	λ_{em} (nm) (77 K)	IQYs (%) 360 nm	CIE	CRI	CCT (K)
2a	pz	0.05	3.0	494 (HE) 545 (LE)	494	60	0.34, 0.41	68.4	5792
2b	pz	0.07	3.0	494 (HE) 545 (LE)	494	64	0.35, 0.42	67.0	5024
2c	pz	0.12	3.0	484 (HE) 545 (LE)	494	61	0.39, 0.43	67.2	3888
2d	pz	0.32	3.0	494 (HE) 545 (LE)	494	54	0.42, 0.46	58.0	3658
2e	2-et-pz	0.12	3.0	494 (HE) 520 (LE)	494	68	0.26, 0.36	65.4	4259
2f	2-me-pz	0.12	3.0	494 (HE) 525 (LE)	494	66	0.28, 0.37	65.5	3940
2g	2-Cl-pz	0.12	3.0	494 (HE) 556 (LE)	494	35	0.43, 0.42	77.2	3697
2h	2-Br-pz	0.12	3.0	494 (HE) 575 (LE)	494	24	0.44, 0.40	75.6	3360

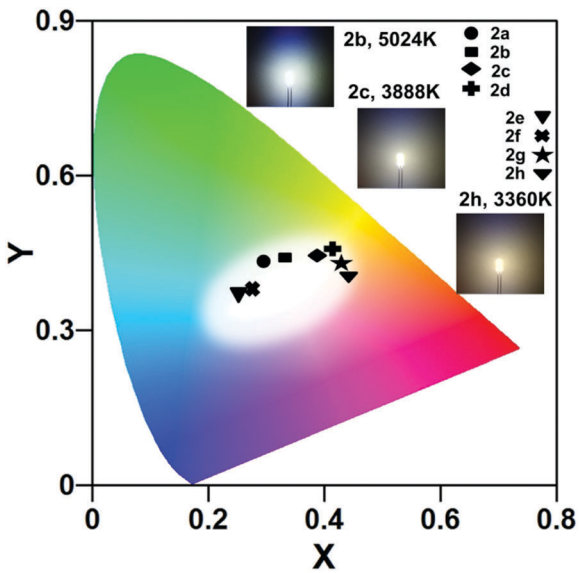

Fig. 4 CIE coordinates of all white-light-emitting structures. Inset: Photos of the LED bulbs under working condition.

(3,5-dm-py, >98%, Alfa Aesar), 3-chloropyridine (3-Cl-py, 99%, Alfa Aesar), 3-bromopyridine (3-Br-py, >98%, Alfa Aesar), pyrazine (pz, 98%, Alfa Aesar), 2-ethyl-pyrazine (2-et-pz, 98%, Alfa Aesar), 2-methyl-pyrazine (2-me-pz, 98%, TCI), 2-chloro-pyrazine (2-Cl-pz, 98%, Alfa Aesar), 2-bromo-pyrazine (2-Br-pz, 98%, TCI), and sodium salicylate (SS, 99%, Merck).

General procedures for the synthesis of undoped structures (1) to (4)

Single crystals of 1D-CuBr(3,5-dm-py) (**1**), 1D-CuBr(py) (**2**), 1D-CuBr(3-Cl-py) (**3**) and 1D-CuBr(3-Br-py) (**4**) were acquired by a layering method. The reactions were conducted in glass vials or tubes (Fig. S1–S3, ESI†). The bottom, middle and top layers were a CuBr/KBr saturated aqueous solution, acetonitrile, and a ligand in ethanol, respectively. The crystals formed in the middle layer over 3–5 days at room temperature. Pure phase powder samples were obtained by direct mixing of CuBr (0.1 mmol) in a saturated KBr solution (2.0 ml) with the ligand (0.1 mmol) in ethanol (2.0 ml). The pure phase powder generally formed immediately after stirring.

General procedures for the synthesis of the doped structures

The synthesis of doped compounds 1D-CuBr(py)$_{1-x}$(pz derivatives)$_x$ ($x < 0.01$) is similar to that of their parent structures. A stock solution of 10^{-4} M pz derivatives in ethanol was pre-prepared. Single crystals of the doped structures were obtained by a layering method. The ligand in an ethanol solution was made by mixing the pz derivative stock solution with py at various molar ratios, from 0% to 1.0% of py. Pure phase powder samples were made by directly mixing the ligand solution with CuBr in a KBr saturated solution while stirring at room temperature. The doped structures obtained are 1D-CuBr(py)$_{1-x}$(pz)$_x$ (x = 0.0005, **2a**; x = 0.0007, **2b**; x = 0.0012, **2c**; x = 0.0032, **2d**) and 1D-CuBr(py)$_{0.9988}$(pz derivatives)$_{0.0012}$, (pz derivatives) = 2-et-pz (**2e**); 2-me-pz (**2f**); 2-Cl-pz (**2g**); and 2-Br-pz (**2h**). All products were collected by filtration and dried in an vacuum oven for further characterization.

Single crystal X-ray diffraction (SXRD) and powder X-ray diffraction (PXRD) analysis

Single crystal X-ray diffraction data of **1**, **3**, and **4** were collected at low temperature (100 K) on a Bruker-AXS smart APEX I CCD diffractometer with graphite-monochromated MoKα radiation (λ = 0.71073 Å) at room temperature. The structures were solved by direct methods and refined by full-matrix least-squares on F2 using the Bruker SHELXTL package. The structures were

deposited in the Cambridge Structural Database (CSD), and the file numbers are 1506741, 1506742, and 1506745.† A summary of the crystal data of all five compounds are given in Table 1. PXRD patterns of these structures were obtained using a Rigaku Ultima-IV automated diffraction system with Cu Kα radiation. Measurements were made in the 2θ range of 3–50°. The data were collected at room temperature with a step size of 0.02° (2θ) and a counting time of 0.2 s/step. The operating power was 40 kV/44 mA.

Characterization and DFT calculations

Optical diffuse reflectance spectra were measured at room temperature on a Shimadzu UV-3600 spectrophotometer. Data were collected in the wavelength range of 300–1000 nm and the % reflectance was converted to the Kubelka–Munk function. Photoluminescence (PL) measurements were carried out on a Varian Cary Eclipse spectrophotometer at room temperature. Thermogravimetric (TG) analyses were performed on a computer-controlled TG Q5000 analyzer (TA Instruments) at a ramp rate of 10 °C min^{-1} from room temperature to 400 °C. The internal quantum yield (IQY) was measured for the samples in the powder form using a C9920-03 absolute quantum yield measurement system (Hamamatsu Photonics) with a 150 W xenon monochromatic light source and a 3.3 inch integrating sphere. Sodium salicylate (99%, Merck) was used as the standard with an IQY value of 60% when excited at 360 nm. The IQY value of the standard was measured to be 65%, indicating an experimental error of less than 10%. The luminescence lifetime was measured using an FLS920 Edinburgh fluorimeter (Edinburgh Instruments, Livingston, United Kingdom) with a microsecond μF900 xenon flash lamp as the excitation source and by time-correlated single photon counting. Instrumental response function (IRF) was applied if the instrumental response could not be neglected for shorter lifetimes.

Conclusions

In summary, a series of copper bromide inorganic–organic hybrid semiconductors have been synthesized and structurally characterized. Upon doping with a trace amount of the second, multidentate ligand, they exhibit bright and tunable white light emissions. The color quality of their white emission can be precisely controlled and tuned by varying the dopant and doping amount, generating a range of "cold" to "warm" emissions. All doped compounds also exhibit thermochromic behavior as a function of temperature. This work provides the first example of a systematic study that demonstrates a dopant effect on the photoluminescence of copper bromide based hybrid structures.

Conflicts of interest

There are no conflicts to declare.

Acknowledgements

Financial support from the National Science Foundation (Grant no. DMR-1507210) is gratefully acknowledged.

Notes and references

1 X. Huang, *Nat. Photonics*, 2014, **8**, 748–749.
2 Y. H. Kim, P. Arunkumar, S. H. Park, H. S. Yoon and W. B. Im, *J. Mater. Sci. Eng. B*, 2015, **193**, 4–12.
3 H. Zhu, C. C. Lin, W. Luo, S. Shu, Z. Liu, Y. Liu, J. Kong, E. Ma, Y. Cao, R.-S. Liu and X. Chen, *Nat. Commun.*, 2014, 5.
4 B. Song, Y. Zhong, S. Wu, B. Chu, Y. Su and Y. He, *J. Am. Chem. Soc.*, 2016, **138**, 4824–4831.
5 N. Horiuchi, *Nat. Photonics*, 2010, **4**, 738.
6 M. Yoshihiko, K. Masahiro and N. Suguru, *Semicond. Sci. Technol.*, 2014, **29**, 084004.
7 N. C. George, K. A. Denault and R. Seshadri, *Annu. Rev. Mater. Res.*, 2013, **43**, 481–501.
8 A. Moazzam, C. Soma, N. Angshuman, K. Akshay, S. Sameer, S. Chakraborty and D. D. Sarma, *Nanotechnology*, 2007, **18**, 075401.
9 P. Thiyagarajan, M. Kottaisamy and M. S. R. Rao, *J. Phys. D: Appl. Phys.*, 2006, **39**, 2701.
10 H. J. Yu, K. Park, W. Chung, J. Kim, B.-H. Chun and S. H. Kim, *Polym. J.*, 2009, **41**, 1076–1079.
11 B. Sprecher, I. Daigo, S. Murakami, R. Kleijn, M. Vos and G. J. Kramer, *Environ. Sci. Technol.*, 2015, **49**, 6740–6750.
12 A. Tukker, *Environ. Sci. Technol.*, 2014, **48**, 9973–9974.
13 Y.-C. Liao, C.-H. Lin and S.-L. Wang, *J. Am. Chem. Soc.*, 2005, **127**, 9986–9987.
14 W. Ki and J. Li, *J. Am. Chem. Soc.*, 2008, **130**, 8114–8115.
15 T. Ogi, H. Iwasaki, A. B. D. Nandiyanto, F. Iskandar, W. N. Wang and K. Okuyama, *J. Mater. Chem. C*, 2014, **2**, 4297–4303.
16 T. Nakajima, M. Isobe, Y. Uzawa and T. Tsuchiya, *J. Mater. Chem. C*, 2015, **3**, 10748–10754.
17 Z.-Y. Mao, F. Wang, J.-J. Chen and D.-J. Wang, *J. Am. Ceram. Soc.*, 2015, **98**, 3856–3862.
18 W. Liu, K. Zhu, S. J. Teat, G. Dey, Z. Shen, L. Wang, D. M. O'Carroll and J. Li, *J. Am. Chem. Soc.*, 2017, **139**, 9281–9290.
19 W. Liu, Y. Fang and J. Li, *Adv. Funct. Mater.*, 2018, **28**, 1705593.
20 M.-S. Wang, S.-P. Guo, Y. Li, L.-Z. Cai, J.-P. Zou, G. Xu, W.-W. Zhou, F.-K. Zheng and G.-C. Guo, *J. Am. Chem. Soc.*, 2009, **131**, 13572–13573.
21 Z.-F. Liu, M.-F. Wu, S.-H. Wang, F.-K. Zheng, G.-E. Wang, J. Chen, Y. Xiao, A. Q. Wu, G.-C. Guo and J.-S. Huang, *J. Mater. Chem. C*, 2013, **1**, 4634–4639.
22 G.-E. Wang, G. Xu, M.-S. Wang, L.-Z. Cai, W.-H. Li and G.-C. Guo, *Chem. Sci.*, 2015, **6**, 7222–7226.
23 M.-S. Wang and G.-C. Guo, *Chem. Commun.*, 2016, **52**, 13194–13204.
24 N.-N. Zhang, C. Sun, X.-M. Jiang, X.-S. Xing, Y. Yan, L.-Z. Cai, M.-S. Wang and G.-C. Guo, *Chem. Commun.*, 2017, **53**, 9269–9272.
25 M.-S. Wang, G.-C. Guo, W.-T. Chen, G. Xu, W.-W. Zhou, K.-J. Wu and J.-S. Huang, *Angew. Chem., Int. Ed.*, 2007, **46**, 3909–3911.
26 T. E. Rosson, S. M. Claiborne, J. R. McBride, B. S. Stratton and S. J. Rosenthal, *J. Am. Chem. Soc.*, 2012, **134**, 8006–8009.
27 M. J. Bowers, Ii, J. R. McBride, M. D. Garrett, J. A. Sammons, A. D. Dukes Iii, M. A. Schreuder, T. L. Watt, A. R. Lupini,

S. J. Pennycook and S. J. Rosenthal, *J. Am. Chem. Soc.*, 2009, **131**, 5730–5731.
28 A. D. Dukes, P. C. Samson, J. D. Keene, L. M. Davis, J. P. Wikswo and S. J. Rosenthal, *J. Phys. Chem. A*, 2011, **115**, 4076–4081.
29 X. Huang, J. Li and H. Fu, *J. Am. Chem. Soc.*, 2000, **122**, 8789–8790.
30 X. Huang and J. Li, *J. Am. Chem. Soc.*, 2007, **129**, 3157–3162.
31 C. R. Kagan, D. B. Mitzi and C. D. Dimitrakopoulos, *Science*, 1999, **286**, 945–947.
32 D. B. Mitzi, S. Wang, C. A. Feild, C. A. Chess and A. M. Guloy, *Science*, 1995, **267**, 1473–1476.
33 X. Zhang, M. Hejazi, S. J. Thiagarajan, W. R. Woerner, D. Banerjee, T. J. Emge, W. Xu, S. J. Teat, Q. Gong, A. Safari, R. Yang, J. B. Parise and J. Li, *J. Am. Chem. Soc.*, 2013, **135**, 17401–17407.
34 X. Huang, M. Roushan, T. J. Emge, W. Bi, S. Thiagarajan, J.-H. Cheng, R. Yang and J. Li, *Angew. Chem., Int. Ed.*, 2009, **48**, 7871–7874.
35 Z.-J. Zhang, G.-C. Guo, G. Xu, M.-L. Fu, J.-P. Zou and J.-S. Huang, *Inorg. Chem.*, 2006, **45**, 10028–10030.
36 G.-E. Wang, G. Xu, B.-W. Liu, M.-S. Wang, M.-S. Yao and G.-C. Guo, *Angew. Chem., Int. Ed.*, 2016, 55.
37 E. R. Dohner, E. T. Hoke and H. I. Karunadasa, *J. Am. Chem. Soc.*, 2014, **136**, 1718–1721.
38 X. Zhang, W. Liu, G. Z. Wei, D. Banerjee, Z. Hu and J. Li, *J. Am. Chem. Soc.*, 2014, **136**, 14230–14236.
39 C. Sun, G. Xu, X.-M. Jiang, G.-E. Wang, P.-Y. Guo, M.-S. Wang and G.-C. Guo, *J. Am. Chem. Soc.*, 2018, **140**, 2805–2811.
40 C. Sun, M.-S. Wang, P.-X. Li and G.-C. Guo, *Angew. Chem., Int. Ed.*, 2017, **56**, 554–558.
41 X. Fang, M. Roushan, R. Zhang, J. Peng, H. Zeng and J. Li, *Chem. Mater.*, 2012, **24**, 1710–1717.
42 M. Roushan, X. Zhang and J. Li, *Angew. Chem., Int. Ed.*, 2012, **51**, 436–439.
43 E. R. Dohner, A. Jaffe, L. R. Bradshaw and H. I. Karunadasa, *J. Am. Chem. Soc.*, 2014, **136**, 13154–13157.
44 M. D. Smith and H. I. Karunadasa, *Acc. Chem. Res.*, 2018, **51**, 619–627.
45 W. Liu, Y. Fang, G. Z. Wei, S. J. Teat, K. Xiong, Z. Hu, W. P. Lustig and J. Li, *J. Am. Chem. Soc.*, 2015, **137**, 9400–9408.
46 Z. Liu, M. F. Qayyum, C. Wu, M. T. Whited, P. I. Djurovich, K. O. Hodgson, B. Hedman, E. I. Solomon and M. E. Thompson, *J. Am. Chem. Soc.*, 2011, **133**, 3700–3703.
47 Z. Liu, J. Qiu, F. Wei, J. Wang, X. Liu, M. G. Helander, S. Rodney, Z. Wang, Z. Bian, Z. Lu, M. E. Thompson and C. Huang, *Chem. Mater.*, 2014, **26**, 2368–2373.
48 P. C. Ford, E. Cariati and J. Bourassa, *Chem. Rev.*, 1999, **99**, 3625–3648.
49 K. Tsuge, Y. Chishina, H. Hashiguchi, Y. Sasaki, M. Kato, S. Ishizaka and N. Kitamura, *Coord. Chem. Rev.*, 2016, **306**(Part 2), 636–651.
50 P. Healy, J. Kildea, B. Skelton and A. White, *Aust. J. Chem.*, 1989, **42**, 93–105.
51 J. Pospisil, I. Jess, C. Nather, M. Necas and P. Taborsky, *New J. Chem.*, 2011, **35**, 861–864.
52 S. Perruchas, C. Tard, X. F. Le Goff, A. Fargues, A. Garcia, S. Kahlal, J.-Y. Saillard, T. Gacoin and J.-P. Boilot, *Inorg. Chem.*, 2011, **50**, 10682–10692.
53 S. Perruchas, X. F. Le Goff, S. Maron, I. Maurin, F. Guillen, A. Garcia, T. Gacoin and J.-P. Boilot, *J. Am. Chem. Soc.*, 2010, **132**, 10967–10969.
54 Q. Benito, X. F. Le Goff, S. Maron, A. Fargues, A. Garcia, C. Martineau, F. Taulelle, S. Kahlal, T. Gacoin, J.-P. Boilot and S. Perruchas, *J. Am. Chem. Soc.*, 2014, **136**, 11311–11320.

